Cloud based spatio-temporal analysis of change in sequences of Sentinel images

Allan A. Nielsen[1], **Morton J. Canty**[2], **Henning Skriver**[1], **Knut Conradsen**[1]

[1]**Technical University of Denmark**
[2]**Research Center Jülich, Germany**

ESA Big Data from Space, Munich, Germany, 19-21 Feb 2019

Outline

- Optical data, bi-temporal change detection and normalization.

Outline

- Optical data, bi-temporal change detection and normalization.
- Radar data, PolSAR, multi-temporal change detection, visualization.

Outline

- Optical data, bi-temporal change detection and normalization.
- Radar data, PolSAR, multi-temporal change detection, visualization.
- Computer implementations, including cloud.

Outline

- Optical data, bi-temporal change detection and normalization.
- Radar data, PolSAR, multi-temporal change detection, visualization.
- Computer implementations, including cloud.
- Ongoing work, here on latest developments (no time to go into optical part).

Optical data

- m dimensional $\boldsymbol{X}$ at t_1 and $\boldsymbol{Y}$ at t_2 with reflected or emitted EM signal.

Optical data

- m dimensional $\boldsymbol{X}$ at t_1 and $\boldsymbol{Y}$ at t_2 with reflected or emitted EM signal.
- Wavelengths λ typically VIS (400-700 nm), NIR, SWIR and TIR (3-15 μm, typically 10-12 μm).

Optical data

- m dimensional $\boldsymbol{X}$ at t_1 and $\boldsymbol{Y}$ at t_2 with reflected or emitted EM signal.
- Wavelengths λ typically VIS (400-700 nm), NIR, SWIR and TIR (3-15 μm, typically 10-12 μm).
- Space- or airborne imaging instruments.

Optical data

- m dimensional $\boldsymbol{X}$ at t_1 and $\boldsymbol{Y}$ at t_2 with reflected or emitted EM signal.
- Wavelengths λ typically VIS (400-700 nm), NIR, SWIR and TIR (3-15 μm, typically 10-12 μm).
- Space- or airborne imaging instruments.
- Detect change in graytone images ($m = 1$): after normalization subtract, $\boldsymbol{X} - \boldsymbol{Y}$. Zero is no-change, large positive and large negative values are change.

Optical data

- Idea to detect change in bitemporal multispectral images $\boldsymbol{X}$ and $\boldsymbol{Y}$ with m spectral bands: after normalization, do bandwise subtractions $\boldsymbol{X} - \boldsymbol{Y}$ and maybe concentrate change information, e.g., $\boldsymbol{v}^T(\boldsymbol{X} - \boldsymbol{Y})$ by PCA or SVD.

Optical data

- Idea to detect change in bitemporal multispectral images $\boldsymbol{X}$ and $\boldsymbol{Y}$ with m spectral bands: after normalization, do bandwise subtractions $\boldsymbol{X} - \boldsymbol{Y}$ and maybe concentrate change information, e.g., $\boldsymbol{v}^T(\boldsymbol{X} - \boldsymbol{Y})$ by PCA or SVD.
- Better idea: (no normalization) do CCA followed by pairwise subtractions of CVs and maybe concentrate change information (MAD method). CCA orders the image bands according to similarity (correlation) rather than spectral wavelength. The differences between corresponding pairs of canonical variates are termed the MAD variates.

Optical data

- Idea to detect change in bitemporal multispectral images $\boldsymbol{X}$ and $\boldsymbol{Y}$ with m spectral bands: after normalization, do bandwise subtractions $\boldsymbol{X} - \boldsymbol{Y}$ and maybe concentrate change information, e.g., $\boldsymbol{v}^T(\boldsymbol{X} - \boldsymbol{Y})$ by PCA or SVD.
- Better idea: (no normalization) do CCA followed by pairwise subtractions of CVs and maybe concentrate change information (MAD method). CCA orders the image bands according to similarity (correlation) rather than spectral wavelength. The differences between corresponding pairs of canonical variates are termed the MAD variates.
- Specifically, a MAD variate Z is

$$Z = \boldsymbol{a}^T\boldsymbol{X} - \boldsymbol{b}^T\boldsymbol{Y}$$

where $\boldsymbol{a}$ and $\boldsymbol{b}$ are the eigenvectors from the CCA.

Optical data

- Thus $\boldsymbol{a}^T\boldsymbol{X}$ is a canonical variate for t_1 and $\boldsymbol{b}^T\boldsymbol{Y}$ is a canonical variate for t_2. We have m uncorrelated canonical variates (CVs) with mean value zero and variance one from both time points, the correlation between corresponding pairs of CVs is ρ (termed the canonical correlation which is maximized in CCA), and we have m uncorrelated MAD variates with variance $2(1-\rho)$.

Optical data

- Thus $\boldsymbol{a}^T\boldsymbol{X}$ is a canonical variate for t_1 and $\boldsymbol{b}^T\boldsymbol{Y}$ is a canonical variate for t_2. We have m uncorrelated canonical variates (CVs) with mean value zero and variance one from both time points, the correlation between corresponding pairs of CVs is ρ (termed the canonical correlation which is maximized in CCA), and we have m uncorrelated MAD variates with variance $2(1-\rho)$.
- Even better: iterate CCA to obtain an increasingly better background of no-change against which to detect change.

Optical data

- In each iteration the values of each image pixel j in $\boldsymbol{X}$ and $\boldsymbol{Y}$ are weighted by w_j which is the current estimate of the no-change probability and the image statistics (mean and covariance matrices) are re-sampled.

Optical data

- In each iteration the values of each image pixel j in $\boldsymbol{X}$ and $\boldsymbol{Y}$ are weighted by w_j which is the current estimate of the no-change probability and the image statistics (mean and covariance matrices) are re-sampled.
- Since the MAD variates for the no-change observations are approximately Gaussian and uncorrelated, the sum of their squared values (after normalization to unit variance)

$$C^2 = \sum_{i=1}^{m} \frac{Z_i^2}{2(1-\rho_i)}$$

will ideally follow a chi squared distribution with m degrees of freedom, $C^2 \sim \chi^2(m)$.

Optical data

- The probability of finding a smaller value of C^2 is approximated by (c^2 is the actually observed value of C^2)

$$P\{C^2 \leq c^2\} \;\simeq\; P\{\chi^2(m) \leq c^2\}.$$

Optical data

- The probability of finding a smaller value of C^2 is approximated by (c^2 is the actually observed value of C^2)

$$P\{C^2 \leq c^2\} \;\simeq\; P\{\chi^2(m) \leq c^2\}.$$

- Hence the no-change probability used as weight w_j in the iterations is

$$w_j \;=\; 1 - P\{\chi^2(m) \leq c^2\}.$$

Optical data

- The probability of finding a smaller value of C^2 is approximated by (c^2 is the actually observed value of C^2)

$$P\{C^2 \leq c^2\} \simeq P\{\chi^2(m) \leq c^2\}.$$

- Hence the no-change probability used as weight w_j in the iterations is

$$w_j = 1 - P\{\chi^2(m) \leq c^2\}.$$

- Iterations continue until the canonical correlations stop changing (or a maximum number of iterations is reached).

Optical data

- The probability of finding a smaller value of C^2 is approximated by (c^2 is the actually observed value of C^2)

$$P\{C^2 \leq c^2\} \simeq P\{\chi^2(m) \leq c^2\}.$$

- Hence the no-change probability used as weight w_j in the iterations is

$$w_j = 1 - P\{\chi^2(m) \leq c^2\}.$$

- Iterations continue until the canonical correlations stop changing (or a maximum number of iterations is reached).
- Orthogonality of the CVs/MADs: discrimination between types of change.

χ^2 distribution

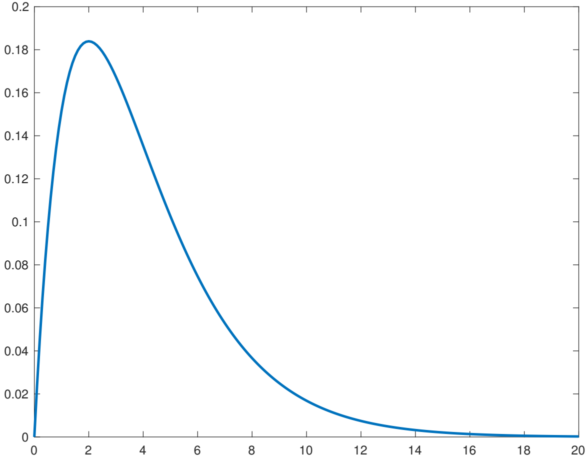

χ^2 distribution with 4 degrees of freedom.

S-2, 4 Apr and 7 July 2017, forest fire, GEE

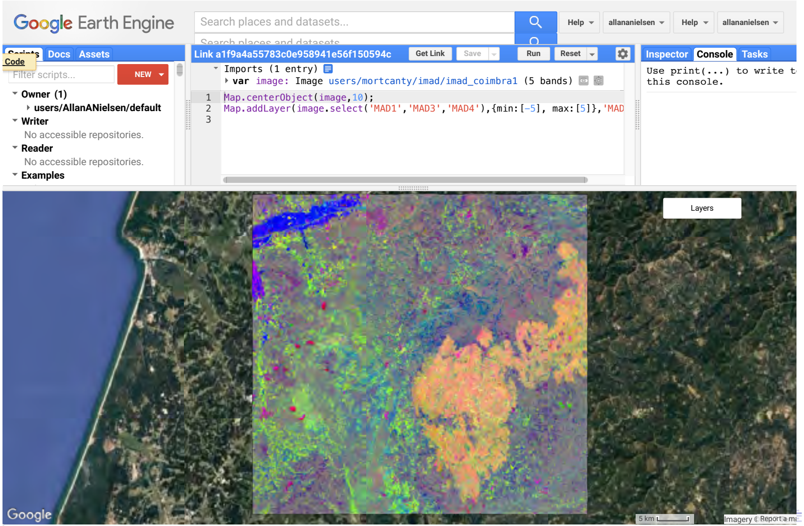

S-2, 20 and 30 Aug 2017, hurricane Harvey, GEE

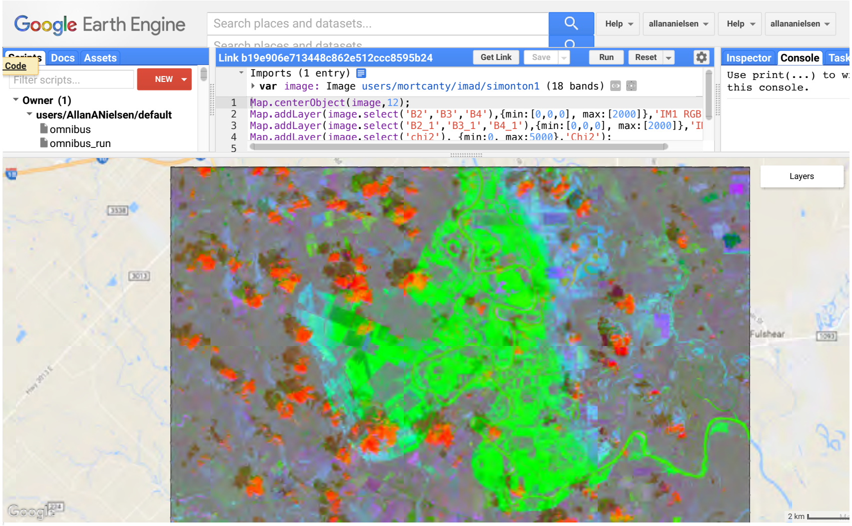

S-2, 5 Oct and 1 Nov, Tubbs Fire, GEE

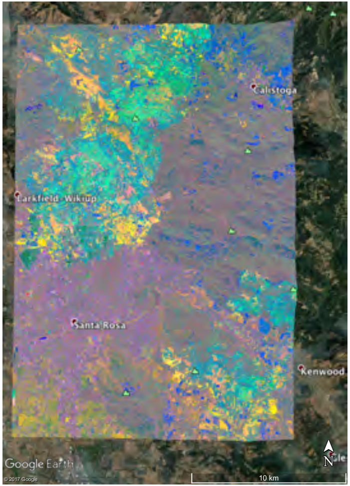

S-2, 5 Oct and 1 Nov, Tubbs Fire, GEE

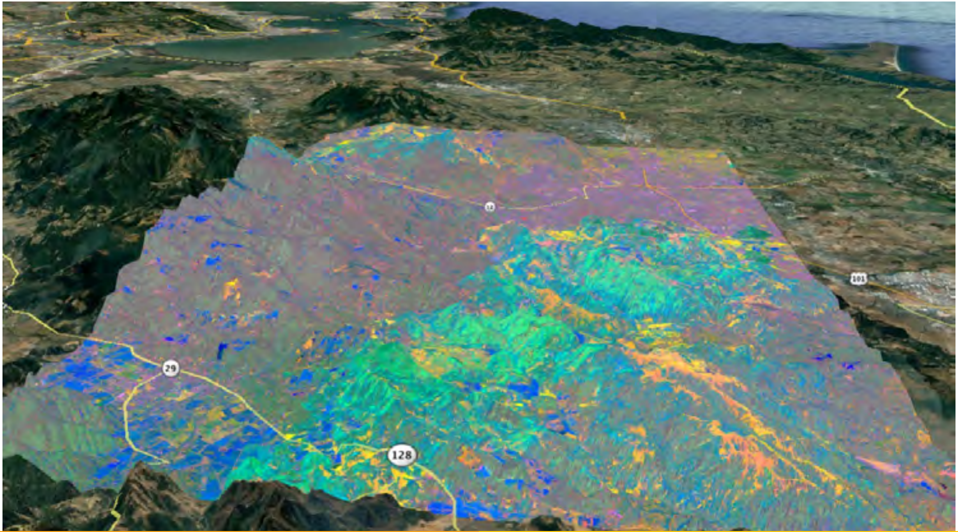

Landsat TM, normalization

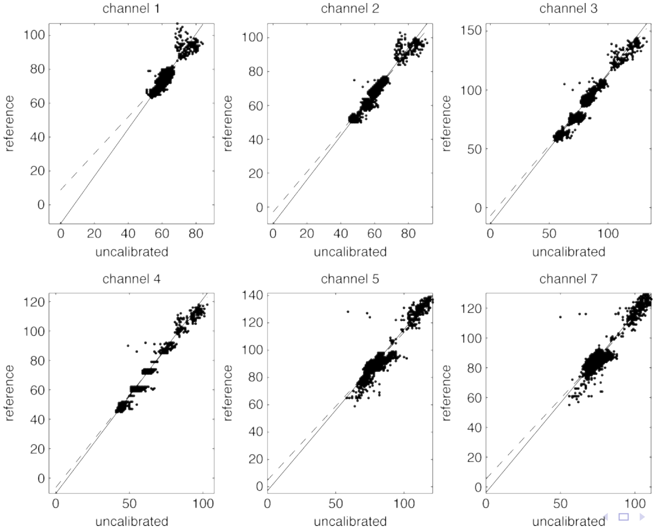

Polarimetric SAR data

- Space- or airborne imaging synthetic aperture radar, SAR. λ typically 3-100 cm (all-weather, day-and-night capability).

Polarimetric SAR data

- Space- or airborne imaging synthetic aperture radar, SAR. λ typically 3-100 cm (all-weather, day-and-night capability).
- PolSAR: transmit and receive horizontally and vertically: $S_{hh}, S_{hv}, S_{vh}, S_{vv}$.

Polarimetric SAR data

- Space- or airborne imaging synthetic aperture radar, SAR. λ typically 3-100 cm (all-weather, day-and-night capability).
- PolSAR: transmit and receive horizontally and vertically: $S_{hh}, S_{hv}, S_{vh}, S_{vv}$.
- Reciprocity: $S_{hv} = S_{vh}$: $\boldsymbol{s} = [S_{hh}\ S_{hv}\ S_{vv}]^T$.

Polarimetric SAR data

- Space- or airborne imaging synthetic aperture radar, SAR. λ typically 3-100 cm (all-weather, day-and-night capability).
- PolSAR: transmit and receive horizontally and vertically: $S_{hh}, S_{hv}, S_{vh}, S_{vv}$.
- Reciprocity: $S_{hv} = S_{vh}$: $\boldsymbol{s} = [S_{hh}\ S_{hv}\ S_{vv}]^T$.
- Coherent pulses: speckle, multilooking.

Polarimetric SAR data

- Space- or airborne imaging synthetic aperture radar, SAR. λ typically 3-100 cm (all-weather, day-and-night capability).
- PolSAR: transmit and receive horizontally and vertically: $S_{hh}, S_{hv}, S_{vh}, S_{vv}$.
- Reciprocity: $S_{hv} = S_{vh}$: $\boldsymbol{s} = [S_{hh}\ S_{hv}\ S_{vv}]^T$.
- Coherent pulses: speckle, multilooking.
- In the covariance matrix representation each pixel at each time point is a matrix $\langle \boldsymbol{C} \rangle$; $\langle \boldsymbol{C} \rangle \times \text{ENL} \sim$ complex Wishart for fully developed speckle

$$
\begin{aligned}
\langle \boldsymbol{C} \rangle_{full} &= \langle \boldsymbol{s}\boldsymbol{s}^H \rangle \\
&= \begin{bmatrix} \langle S_{hh}S_{hh}^* \rangle & \langle S_{hh}S_{hv}^* \rangle & \langle S_{hh}S_{vv}^* \rangle \\ \langle S_{hv}S_{hh}^* \rangle & \langle S_{hv}S_{hv}^* \rangle & \langle S_{hv}S_{vv}^* \rangle \\ \langle S_{vv}S_{hh}^* \rangle & \langle S_{vv}S_{hv}^* \rangle & \langle S_{vv}S_{vv}^* \rangle \end{bmatrix}.
\end{aligned}
$$

Polarimetric SAR data

- Detect change in a series of k full/quad pol, multi-looked SAR data sets in the covariance representation.

Polarimetric SAR data

- Detect change in a series of k full/quad pol, multi-looked SAR data sets in the covariance representation.
- Omnibus likelihood ratio test statistic Q for the equality of several variance-covariance matrices following the complex Wishart distribution; Q establishes if change occurs.

Polarimetric SAR data

- Detect change in a series of k full/quad pol, multi-looked SAR data sets in the covariance representation.
- Omnibus likelihood ratio test statistic Q for the equality of several variance-covariance matrices following the complex Wishart distribution; Q establishes if change occurs.
- Associated p-value for Q under equality hypothesis.

Polarimetric SAR data

- Detect change in a series of k full/quad pol, multi-looked SAR data sets in the covariance representation.
- Omnibus likelihood ratio test statistic Q for the equality of several variance-covariance matrices following the complex Wishart distribution; Q establishes if change occurs.
- Associated p-value for Q under equality hypothesis.
- Factorization of $Q = \prod_2^k R_j$; if change occurs, R_j establishes when.

Polarimetric SAR data

- Detect change in a series of k full/quad pol, multi-looked SAR data sets in the covariance representation.
- Omnibus likelihood ratio test statistic Q for the equality of several variance-covariance matrices following the complex Wishart distribution; Q establishes if change occurs.
- Associated p-value for Q under equality hypothesis.
- Factorization of $Q = \prod_2^k R_j$; if change occurs, R_j establishes when.
- Associated p-value for R_j.

Polarimetric SAR data, full

- H_0 : no change between all k time points $(\boldsymbol{\Sigma}_1 = \boldsymbol{\Sigma}_2 = \cdots = \boldsymbol{\Sigma}_k)$

$$\ln Q \quad = \quad n\{pk \ln k + \sum_{i=1}^{k} \ln |\boldsymbol{X}_i| - k \ln |\sum_{i=1}^{k} \boldsymbol{X}_i|\} \tag{1}$$

$p = 3$, $\boldsymbol{X}_i = n\langle \boldsymbol{C} \rangle_{full}$, n is ENL, the equivalent number of looks, and $|\cdot|$ denotes the determinant.[1]

[1] K. Conradsen, A. A. Nielsen, and H. Skriver (2016), Determining the points of change in time series of polarimetric SAR data. *IEEE Transactions on Geoscience and Remote Sensing* **54**(5), 3007-3024. http://www.imm.dtu.dk/pubdb/p.php?6825

Polarimetric SAR data, full

- H_0 : no change between all k time points $(\boldsymbol{\Sigma}_1 = \boldsymbol{\Sigma}_2 = \cdots = \boldsymbol{\Sigma}_k)$

$$\ln Q = n\{pk \ln k + \sum_{i=1}^{k} \ln |\boldsymbol{X}_i| - k \ln |\sum_{i=1}^{k} \boldsymbol{X}_i|\} \quad (1)$$

$p = 3$, $\boldsymbol{X}_i = n\langle \boldsymbol{C} \rangle_{full}$, n is ENL, the equivalent number of looks, and $|\cdot|$ denotes the determinant.[1]

- Under H_0, $-2 \ln Q \sim \chi^2((k-1)f)$:
  $P\{-2 \ln Q \leq z\} = P\{\chi^2((k-1)f) \leq z\}$, $z = -2 \ln q_{\text{obs}}$, $f = p^2 = 9$.

[1] K. Conradsen, A. A. Nielsen, and H. Skriver (2016), Determining the points of change in time series of polarimetric SAR data. *IEEE Transactions on Geoscience and Remote Sensing* **54**(5), 3007-3024. `http://www.imm.dtu.dk/pubdb/p.php?6825`

Polarimetric SAR data, full

- H_0 : no change between all k time points ($\boldsymbol{\Sigma}_1 = \boldsymbol{\Sigma}_2 = \cdots = \boldsymbol{\Sigma}_k$)

$$\ln Q = n\{pk \ln k + \sum_{i=1}^{k} \ln |\boldsymbol{X}_i| - k \ln |\sum_{i=1}^{k} \boldsymbol{X}_i|\} \tag{1}$$

$p = 3$, $\boldsymbol{X}_i = n\langle \boldsymbol{C} \rangle_{full}$, n is ENL, the equivalent number of looks, and $|\cdot|$ denotes the determinant.[1]

- Under H_0, $-2 \ln Q \sim \chi^2((k-1)f)$:
  $P\{-2 \ln Q \leq z\} = P\{\chi^2((k-1)f) \leq z\}$, $z = -2 \ln q_{\rm obs}$, $f = p^2 = 9$.
- Better approximation for $P\{-2\rho \ln Q \leq z\}$ (ρ is auxiliary variable).

[1] K. Conradsen, A. A. Nielsen, and H. Skriver (2016), Determining the points of change in time series of polarimetric SAR data. *IEEE Transactions on Geoscience and Remote Sensing* **54**(5), 3007-3024. `http://www.imm.dtu.dk/pubdb/p.php?6825`

Polarimetric SAR data, full

- If there is change (we reject H_0), to find when, test whether the first j $(1 < j \leq k)$ complex variance-covariance matrices $\mathbf{\Sigma}_i$ are equal, i.e., $H_{0,j}$: given that $\mathbf{\Sigma}_1 = \mathbf{\Sigma}_2 = \cdots = \mathbf{\Sigma}_{j-1}$, $\mathbf{\Sigma}_j = \mathbf{\Sigma}_1$

$$\begin{aligned} \ln R_j &= n\{p(j \ln j - (j-1)\ln(j-1)) \\ &\quad + (j-1)\ln|\sum_{i=1}^{j-1} \boldsymbol{X}_i| + \ln|\boldsymbol{X}_j| - j\ln|\sum_{i=1}^{j} \boldsymbol{X}_i|\}. \end{aligned} \tag{2}$$

Polarimetric SAR data, full

- If there is change (we reject H_0), to find when, test whether the first j $(1 < j \leq k)$ complex variance-covariance matrices $\mathbf{\Sigma}_i$ are equal, i.e., $H_{0,j}$: given that $\mathbf{\Sigma}_1 = \mathbf{\Sigma}_2 = \cdots = \mathbf{\Sigma}_{j-1}$, $\mathbf{\Sigma}_j = \mathbf{\Sigma}_1$

$$\begin{aligned} \ln R_j &= n\{p(j \ln j - (j-1)\ln(j-1)) \\ &\quad + (j-1)\ln|\sum_{i=1}^{j-1} \boldsymbol{X}_i| + \ln|\boldsymbol{X}_j| - j\ln|\sum_{i=1}^{j} \boldsymbol{X}_i|\}. \end{aligned} \tag{2}$$

- Under $H_{0,j}$, $-2\ln R_j \;\sim\; \chi^2(f)$:
  $P\{-2\ln R_j \leq z_j\} = P\{\chi^2(f) \leq z_j\}$, $z_j = -2\ln r_{j,\mathrm{obs}}$, $f = p^2 = 9$.

Polarimetric SAR data, full

- If there is change (we reject H_0), to find when, test whether the first j $(1 < j \leq k)$ complex variance-covariance matrices $\boldsymbol{\Sigma}_i$ are equal, i.e., $H_{0,j}$: given that $\boldsymbol{\Sigma}_1 = \boldsymbol{\Sigma}_2 = \cdots = \boldsymbol{\Sigma}_{j-1}$, $\boldsymbol{\Sigma}_j = \boldsymbol{\Sigma}_1$

$$\begin{aligned} \ln R_j &= n\{p(j \ln j - (j-1)\ln(j-1)) \\ &\quad + (j-1)\ln|\sum_{i=1}^{j-1} \boldsymbol{X}_i| + \ln|\boldsymbol{X}_j| - j \ln|\sum_{i=1}^{j} \boldsymbol{X}_i|\}. \end{aligned} \tag{2}$$

- Under $H_{0,j}$, $-2\ln R_j \sim \chi^2(f)$: $P\{-2\ln R_j \leq z_j\} = P\{\chi^2(f) \leq z_j\}$, $z_j = -2\ln r_{j,\text{obs}}$, $f = p^2 = 9$.
- Better approximation for $P\{-2\rho_j \ln R_j \leq z_j\}$ (ρ_j are auxiliary variables).

Polarimetric SAR data, full

- If there is change (we reject H_0), to find when, test whether the first j $(1 < j \leq k)$ complex variance-covariance matrices $\boldsymbol{\Sigma}_i$ are equal, i.e., $H_{0,j}$: given that $\boldsymbol{\Sigma}_1 = \boldsymbol{\Sigma}_2 = \cdots = \boldsymbol{\Sigma}_{j-1}$, $\boldsymbol{\Sigma}_j = \boldsymbol{\Sigma}_1$

$$\begin{aligned} \ln R_j &= n\{p(j \ln j - (j-1)\ln(j-1)) \\ &\quad + (j-1)\ln|\sum_{i=1}^{j-1} \boldsymbol{X}_i| + \ln|\boldsymbol{X}_j| - j\ln|\sum_{i=1}^{j} \boldsymbol{X}_i|\}. \end{aligned} \tag{2}$$

- Under $H_{0,j}$, $-2\ln R_j \;\sim\; \chi^2(f)$: $P\{-2\ln R_j \leq z_j\} = P\{\chi^2(f) \leq z_j\}$, $z_j = -2\ln r_{j,\text{obs}}$, $f = p^2 = 9$.
- Better approximation for $P\{-2\rho_j \ln R_j \leq z_j\}$ (ρ_j are auxiliary variables).
- R_j constitute a factorization $Q = \prod_{j=2}^{k} R_j$ or

$$\ln Q = \sum_{j=2}^{k} \ln R_j. \tag{3}$$

Polarimetric SAR data, dual

- For dual polarimetry, we have for example $\langle \boldsymbol{C} \rangle$; $\langle \boldsymbol{C} \rangle \times \mathrm{ENL} \sim$ complex Wishart for fully developed speckle

$$\langle \boldsymbol{C} \rangle_{dual} = \begin{bmatrix} \langle S_{vv} S_{vv}^* \rangle & \langle S_{vv} S_{vh}^* \rangle \\ \langle S_{vh} S_{vv}^* \rangle & \langle S_{vh} S_{vh}^* \rangle \end{bmatrix}.$$

Polarimetric SAR data, dual

- For dual polarimetry, we have for example $\langle C \rangle$; $\langle C \rangle \times \text{ENL} \sim$ complex Wishart for fully developed speckle

$$\langle C \rangle_{dual} = \begin{bmatrix} \langle S_{vv} S_{vv}^* \rangle & \langle S_{vv} S_{vh}^* \rangle \\ \langle S_{vh} S_{vv}^* \rangle & \langle S_{vh} S_{vh}^* \rangle \end{bmatrix}.$$

- We may think of VV/VH data as the diagonal elements only

$$\langle C \rangle_{dual,diag} = \begin{bmatrix} \langle S_{vv} S_{vv}^* \rangle & 0 \\ 0 & \langle S_{vh} S_{vh}^* \rangle \end{bmatrix};$$

$\langle C \rangle \times \text{ENL}$ not complex Wishart but the two (1 by 1) "blocks" on the diagonal are, $\langle S_{vv} S_{vv}^* \rangle$ is 1 by 1, $p_1 = 1$, and $\langle S_{vh} S_{vh}^* \rangle$ is 1 by 1, $p_2 = 1$.

Polarimetric SAR data, dual

- H_0 : no change between all k time points $(\boldsymbol{\Sigma}_1 = \boldsymbol{\Sigma}_2 = \cdots = \boldsymbol{\Sigma}_k)$

$$\ln Q = n\{pk \ln k + \sum_{i=1}^{k} \ln |\boldsymbol{X}_i| - k \ln |\sum_{i=1}^{k} \boldsymbol{X}_i|\} \quad (4)$$

$p = p_1 + p_2 = 2$, $\boldsymbol{X}_i = n\langle \boldsymbol{C} \rangle_{dual,diag}$, n is ENL, the equivalent number of looks, and $|\cdot|$ denotes the determinant.

Polarimetric SAR data, dual

- H_0 : no change between all k time points ($\boldsymbol{\Sigma}_1 = \boldsymbol{\Sigma}_2 = \cdots = \boldsymbol{\Sigma}_k$)

$$\ln Q \quad = \quad n\{pk \ln k + \sum_{i=1}^{k} \ln |\boldsymbol{X}_i| - k \ln |\sum_{i=1}^{k} \boldsymbol{X}_i|\} \tag{4}$$

  $p = p_1 + p_2 = 2$, $\boldsymbol{X}_i = n\langle \boldsymbol{C} \rangle_{dual,diag}$, n is ENL, the equivalent number of looks, and $|\cdot|$ denotes the determinant.
- Under H_0, $-2 \ln Q \ \sim \ \chi^2((k-1)f)$:
  $P\{-2 \ln Q \leq z\} = P\{\chi^2((k-1)f) \leq z\}$, $z = -2 \ln q_{obs}$, $f = p_1^2 + p_2^2 = 2$.

Polarimetric SAR data, dual

- H_0 : no change between all k time points $(\boldsymbol{\Sigma}_1 = \boldsymbol{\Sigma}_2 = \cdots = \boldsymbol{\Sigma}_k)$

$$\ln Q = n\{pk \ln k + \sum_{i=1}^{k} \ln |\boldsymbol{X}_i| - k \ln |\sum_{i=1}^{k} \boldsymbol{X}_i|\} \tag{4}$$

  $p = p_1 + p_2 = 2$, $\boldsymbol{X}_i = n\langle \boldsymbol{C} \rangle_{dual,diag}$, n is ENL, the equivalent number of looks, and $|\cdot|$ denotes the determinant.
- Under H_0, $-2 \ln Q \sim \chi^2((k-1)f)$:
  $P\{-2 \ln Q \leq z\} = P\{\chi^2((k-1)f) \leq z\}$, $z = -2 \ln q_{obs}$, $f = p_1^2 + p_2^2 = 2$.
- (Better approximation for $P\{-2\rho \ln Q \leq z\}$ (ρ is auxiliary variable)).

Polarimetric SAR data, dual

- If there is change (we reject H_0), to find when, test whether the first j ($1 < j \leq k$) complex variance-covariance matrices $\mathbf{\Sigma}_i$ are equal, i.e., $H_{0,j}$: given that $\mathbf{\Sigma}_1 = \mathbf{\Sigma}_2 = \cdots = \mathbf{\Sigma}_{j-1}$, $\mathbf{\Sigma}_j = \mathbf{\Sigma}_1$

$$\begin{aligned} \ln R_j &= n\{p(j \ln j - (j-1)\ln(j-1)) \\ &\quad + (j-1)\ln|\sum_{i=1}^{j-1} \boldsymbol{X}_i| + \ln|\boldsymbol{X}_j| - j\ln|\sum_{i=1}^{j} \boldsymbol{X}_i|\}. \end{aligned} \tag{5}$$

Polarimetric SAR data, dual

- If there is change (we reject H_0), to find when, test whether the first j $(1 < j \leq k)$ complex variance-covariance matrices $\mathbf{\Sigma}_i$ are equal, i.e., $H_{0,j}$: given that $\mathbf{\Sigma}_1 = \mathbf{\Sigma}_2 = \cdots = \mathbf{\Sigma}_{j-1}$, $\mathbf{\Sigma}_j = \mathbf{\Sigma}_1$

$$\begin{aligned} \ln R_j &= n\{p(j \ln j - (j-1)\ln(j-1)) \\ &\quad + (j-1)\ln|\sum_{i=1}^{j-1} \boldsymbol{X}_i| + \ln|\boldsymbol{X}_j| - j\ln|\sum_{i=1}^{j} \boldsymbol{X}_i|\}. \end{aligned} \tag{5}$$

- Under $H_{0,j}$, $-2\ln R_j \;\sim\; \chi^2(f)$: $P\{-2\ln R_j \leq z_j\} = P\{\chi^2(f) \leq z_j\}$, $z_j = -2\ln r_{j,obs}$, $f = p_1^2 + p_2^2 = 2$.

Polarimetric SAR data, dual

- If there is change (we reject H_0), to find when, test whether the first j $(1 < j \leq k)$ complex variance-covariance matrices $\boldsymbol{\Sigma}_i$ are equal, i.e., $H_{0,j}$: given that $\boldsymbol{\Sigma}_1 = \boldsymbol{\Sigma}_2 = \cdots = \boldsymbol{\Sigma}_{j-1}$, $\boldsymbol{\Sigma}_j = \boldsymbol{\Sigma}_1$

$$\begin{aligned} \ln R_j &= n\{p(j \ln j - (j-1)\ln(j-1)) \\ &\quad + (j-1)\ln\left|\sum_{i=1}^{j-1} \boldsymbol{X}_i\right| + \ln|\boldsymbol{X}_j| - j\ln\left|\sum_{i=1}^{j} \boldsymbol{X}_i\right|\}. \end{aligned} \tag{5}$$

- Under $H_{0,j}$, $-2\ln R_j \;\sim\; \chi^2(f)$:
  $P\{-2\ln R_j \leq z_j\} = P\{\chi^2(f) \leq z_j\}$, $z_j = -2\ln r_{j,obs}$, $f = p_1^2 + p_2^2 = 2$.
- (Better approximation for $P\{-2\rho_j \ln R_j \leq z\}$ (ρ_j are auxiliary variables)).

Polarimetric SAR data, dual

- If there is change (we reject H_0), to find when, test whether the first j $(1 < j \leq k)$ complex variance-covariance matrices $\boldsymbol{\Sigma}_i$ are equal, i.e., $H_{0,j}$: given that $\boldsymbol{\Sigma}_1 = \boldsymbol{\Sigma}_2 = \cdots = \boldsymbol{\Sigma}_{j-1}$, $\boldsymbol{\Sigma}_j = \boldsymbol{\Sigma}_1$

$$\begin{aligned} \ln R_j &= n\{p(j \ln j - (j-1)\ln(j-1)) \\ &\quad + (j-1)\ln|\sum_{i=1}^{j-1} \boldsymbol{X}_i| + \ln|\boldsymbol{X}_j| - j \ln|\sum_{i=1}^{j} \boldsymbol{X}_i|\}. \end{aligned} \tag{5}$$

- Under $H_{0,j}$, $-2\ln R_j \sim \chi^2(f)$: $P\{-2\ln R_j \leq z_j\} = P\{\chi^2(f) \leq z_j\}$, $z_j = -2\ln r_{j,obs}$, $f = p_1^2 + p_2^2 = 2$.
- (Better approximation for $P\{-2\rho_j \ln R_j \leq z\}$ (ρ_j are auxiliary variables)).
- R_j constitute a factorization $Q = \prod_{j=2}^{k} R_j$ or

$$\ln Q = \sum_{j=2}^{k} \ln R_j. \tag{6}$$

Change Structure

Illustration of the change structure for each pixel/patch from seven time points.

	$t_1 = \cdots = t_7$	$t_2 = \cdots = t_7$	$t_3 = \cdots = t_7$	$t_4 = \cdots = t_7$	$t_5 = t_6 = t_7$	$t_6 = t_7$
Omnibus	$Q^{(1)}$	$Q^{(2)}$	$Q^{(3)}$	$Q^{(4)}$	$Q^{(5)}$	$Q^{(6)}$
$t_1 = t_2$	$R_2^{(1)}$					
$t_2 = t_3$	$R_3^{(1)}$	$R_2^{(2)}$				
$t_3 = t_4$	$R_4^{(1)}$	$R_3^{(2)}$	$R_2^{(3)}$			
$t_4 = t_5$	$R_5^{(1)}$	$R_4^{(2)}$	$R_3^{(3)}$	$R_2^{(4)}$		
$t_5 = t_6$	$R_6^{(1)}$	$R_5^{(2)}$	$R_4^{(3)}$	$R_3^{(4)}$	$R_2^{(5)}$	
$t_6 = t_7$	$R_7^{(1)}$	$R_6^{(2)}$	$R_5^{(3)}$	$R_4^{(4)}$	$R_3^{(5)}$	$R_2^{(6)}$

Change Structure

Example of the change structure for each pixel from seven time points.

	$t_1 = \cdots = t_7$	$t_2 = \cdots = t_7$	$t_3 = \cdots = t_7$	$t_4 = \cdots = t_7$	$t_5 = t_6 = t_7$	$t_6 = t_7$
Omnibus	$Q^{(1)}$	$Q^{(2)}$	$Q^{(3)}$	$Q^{(4)}$	$Q^{(5)}$	$Q^{(6)}$
$t_1 = t_2$	$R_2^{(1)}$					
$t_2 = t_3$	$R_3^{(1)}$	$R_2^{(2)}$				
$t_3 = t_4$	$R_4^{(1)}$	$R_3^{(2)}$	$R_2^{(3)}$			
$t_4 = t_5$	$R_5^{(1)}$	$R_4^{(2)}$	$R_3^{(3)}$	$R_2^{(4)}$		
$t_5 = t_6$	$R_6^{(1)}$	$R_5^{(2)}$	$R_4^{(3)}$	$R_3^{(4)}$	$R_2^{(5)}$	
$t_6 = t_7$	$R_7^{(1)}$	$R_6^{(2)}$	$R_5^{(3)}$	$R_4^{(4)}$	$R_3^{(5)}$	$R_2^{(6)}$

Change Structure

Example of the change structure for each pixel from seven time points.

	$t_1 = \cdots = t_7$	$t_2 = \cdots = t_7$	$t_3 = \cdots = t_7$	$t_4 = \cdots = t_7$	$t_5 = t_6 = t_7$	$t_6 = t_7$
Omnibus	$Q^{(1)}$			$Q^{(4)}$		
$t_1 = t_2$	$R_2^{(1)}$					
$t_2 = t_3$	$R_3^{(1)}$					
$t_3 = t_4$	$R_4^{(1)}$					
$t_4 = t_5$				$R_2^{(4)}$		
$t_5 = t_6$				$R_3^{(4)}$		
$t_6 = t_7$						$R_2^{(6)}$

Change Structure

Example of the change structure for each pixel from seven time points (may skip $Q^{(\ell)}$).

	$t_1 = \cdots = t_7$	$t_4 = \cdots = t_7$	$t_6 = t_7$
Omnibus	$Q^{(1)}$	$Q^{(4)}$	
$t_1 = t_2$	$R_2^{(1)}$		
$t_2 = t_3$	$R_3^{(1)}$		
$t_3 = t_4$	$R_4^{(1)}$		
$t_4 = t_5$		$R_2^{(4)}$	
$t_5 = t_6$		$R_3^{(4)}$	
$t_6 = t_7$			$R_2^{(6)}$

Change Structure

$\boxed{R_2^{(\ell)}}$ are the consecutive pair-wise test statistics.

	$t_1 = \cdots = t_7$	$t_2 = \cdots = t_7$	$t_3 = \cdots = t_7$	$t_4 = \cdots = t_7$	$t_5 = t_6 = t_7$	$t_6 = t_7$
Omnibus	$Q^{(1)}$	$Q^{(2)}$	$Q^{(3)}$	$Q^{(4)}$	$Q^{(5)}$	$Q^{(6)}$
$t_1 = t_2$	$\boxed{R_2^{(1)}}$					
$t_2 = t_3$	$R_3^{(1)}$	$\boxed{R_2^{(2)}}$				
$t_3 = t_4$	$R_4^{(1)}$	$R_3^{(2)}$	$\boxed{R_2^{(3)}}$			
$t_4 = t_5$	$R_5^{(1)}$	$R_4^{(2)}$	$R_3^{(3)}$	$\boxed{R_2^{(4)}}$		
$t_5 = t_6$	$R_6^{(1)}$	$R_5^{(2)}$	$R_4^{(3)}$	$R_3^{(4)}$	$\boxed{R_2^{(5)}}$	
$t_6 = t_7$	$R_7^{(1)}$	$R_6^{(2)}$	$R_5^{(3)}$	$R_4^{(4)}$	$R_3^{(5)}$	$\boxed{R_2^{(6)}}$

Data Sentinel-1

- S-1 data acquired in instrument Interferometric Wide Swath (IW) mode, are Ground Range Detected (GRD) scenes, processed using the Sentinel-1 Toolbox[2] to generate a calibrated, ortho-corrected product.

[2] https://sentinel.esa.int/web/sentinel/toolboxes/sentinel-1

Data Sentinel-1

- S-1 data acquired in instrument Interferometric Wide Swath (IW) mode, are Ground Range Detected (GRD) scenes, processed using the Sentinel-1 Toolbox[2] to generate a calibrated, ortho-corrected product.
- Includes thermal noise removal, radiometric calibration, and terrain correction using Shuttle Radar Topography Mission 30 m (SRTM 30) data.

[2] https://sentinel.esa.int/web/sentinel/toolboxes/sentinel-1

Data Sentinel-1

- S-1 data acquired in instrument Interferometric Wide Swath (IW) mode, are Ground Range Detected (GRD) scenes, processed using the Sentinel-1 Toolbox[2] to generate a calibrated, ortho-corrected product.
- Includes thermal noise removal, radiometric calibration, and terrain correction using Shuttle Radar Topography Mission 30 m (SRTM 30) data.
- Used to include saturating the data (quoting GEE): "Values are then clamped to the 1st and 99th percentile to preserve the dynamic range against anomalous outliers, and quantized to 16 bits." GEE is re-ingesting the entire S-1 series in floats.

[2] https://sentinel.esa.int/web/sentinel/toolboxes/sentinel-1

Data Sentinel-1

- S-1 data acquired in instrument Interferometric Wide Swath (IW) mode, are Ground Range Detected (GRD) scenes, processed using the Sentinel-1 Toolbox[2] to generate a calibrated, ortho-corrected product.
- Includes thermal noise removal, radiometric calibration, and terrain correction using Shuttle Radar Topography Mission 30 m (SRTM 30) data.
- Used to include saturating the data (quoting GEE): "Values are then clamped to the 1st and 99th percentile to preserve the dynamic range against anomalous outliers, and quantized to 16 bits." GEE is re-ingesting the entire S-1 series in floats.
- The spatial resolution is (range by azimuth) 20 m by 22 m and the pixel spacing is 10 m.

[2] https://sentinel.esa.int/web/sentinel/toolboxes/sentinel-1

Data Sentinel-1

- S-1 data acquired in instrument Interferometric Wide Swath (IW) mode, are Ground Range Detected (GRD) scenes, processed using the Sentinel-1 Toolbox[2] to generate a calibrated, ortho-corrected product.
- Includes thermal noise removal, radiometric calibration, and terrain correction using Shuttle Radar Topography Mission 30 m (SRTM 30) data.
- Used to include saturating the data (quoting GEE): "Values are then clamped to the 1st and 99th percentile to preserve the dynamic range against anomalous outliers, and quantized to 16 bits." GEE is re-ingesting the entire S-1 series in floats.
- The spatial resolution is (range by azimuth) 20 m by 22 m and the pixel spacing is 10 m.
- The IW data are multi-looked, the number of looks is 5 by 1 and the equivalent number of looks is 4.4 (was 4.9?). VV, VH, covariance matrix representation, diagonal only.

[2] `https://sentinel.esa.int/web/sentinel/toolboxes/sentinel-1`

Data Sentinel-1

- Sentinel-1 dual polarization C-band SAR instrument (here VV/VH, multi-look, covariance representation, diagonal only – from Google Earth Engine, GEE[3]).

[3] https://earthengine.google.com and https://developers.google.com/earth-engine

Data Sentinel-1

- Sentinel-1 dual polarization C-band SAR instrument (here VV/VH, multi-look, covariance representation, diagonal only – from Google Earth Engine, GEE[3]).
- 17 scenes (all ascending node and all with relative orbit number 15), international airport in Frankfurt, Germany (made especially by GEE for our experiments).

[3] https://earthengine.google.com and https://developers.google.com/earth-engine

Data Sentinel-1

- Sentinel-1 dual polarization C-band SAR instrument (here VV/VH, multi-look, covariance representation, diagonal only – from Google Earth Engine, GEE[3]).
- 17 scenes (all ascending node and all with relative orbit number 15), international airport in Frankfurt, Germany (made especially by GEE for our experiments).
- Acquisition dates are from 5 Mar till 31 Oct 2016.

[3] `https://earthengine.google.com` and `https://developers.google.com/earth-engine`

Data Sentinel-1

- Sentinel-1 dual polarization C-band SAR instrument (here VV/VH, multi-look, covariance representation, diagonal only – from Google Earth Engine, GEE[3]).
- 17 scenes (all ascending node and all with relative orbit number 15), international airport in Frankfurt, Germany (made especially by GEE for our experiments).
- Acquisition dates are from 5 Mar till 31 Oct 2016.
- Will show different ways of visualizing change (not all ways are necessarily informative in all applications).

[3] https://earthengine.google.com and https://developers.google.com/earth-engine

Data Sentinel-1

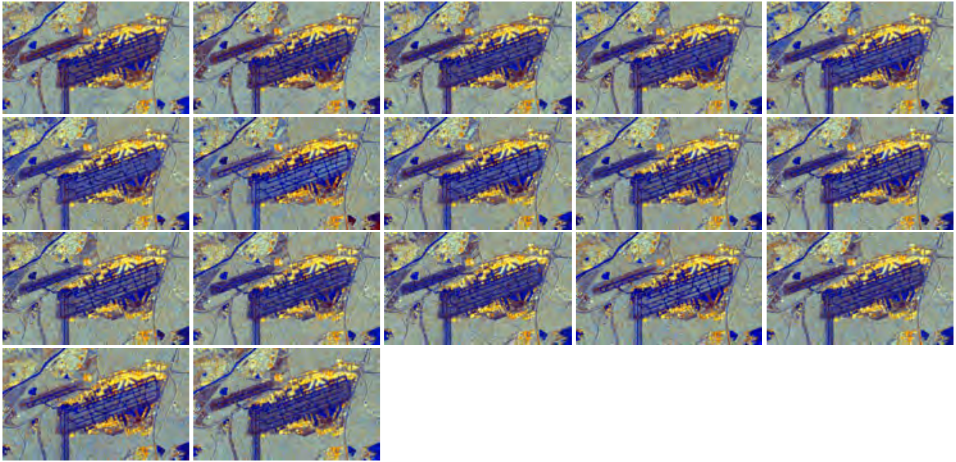

RGB image of Sentinel-1 C-band multi-temporal data, VV as R, VH as G and VH/VV as B, 5 Mar to 31 Oct 2016 as R, 10 m pixels, 6 km north-south and 10 km east-west.

Data Sentinel-1, temporally de-speckled

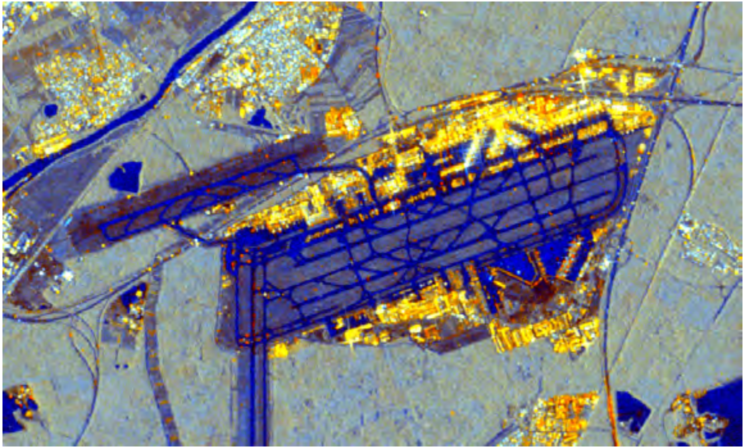

RGB image of temporal mean of all 17 Sentinel-1 C-band VV as R, VH as G and VH/VV as B, 10 m pixels, 6 km north-south and 10 km east-west.

Data Sentinel-2

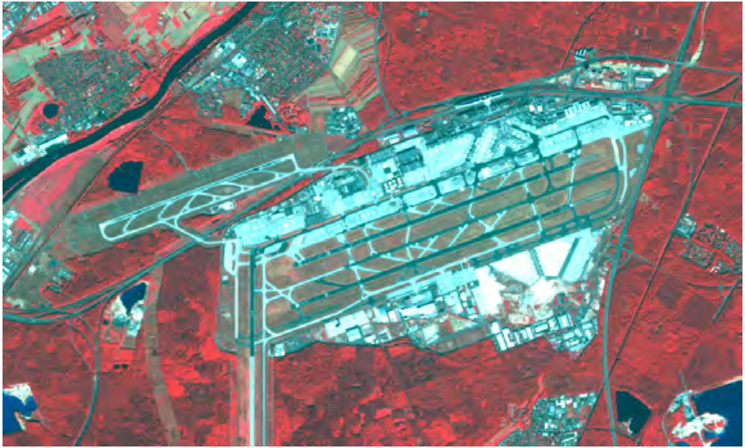

RGB image of Sentinel-2 MSI band 8 (near-infrared as R), band 4 (red as G), and band 3 (green as B), 10 m pixels, 6 km north-south and 10 km east-west, Frankfurt Airport, Germany, acquired on 12 Sep 2016.

Data Sentinel-1

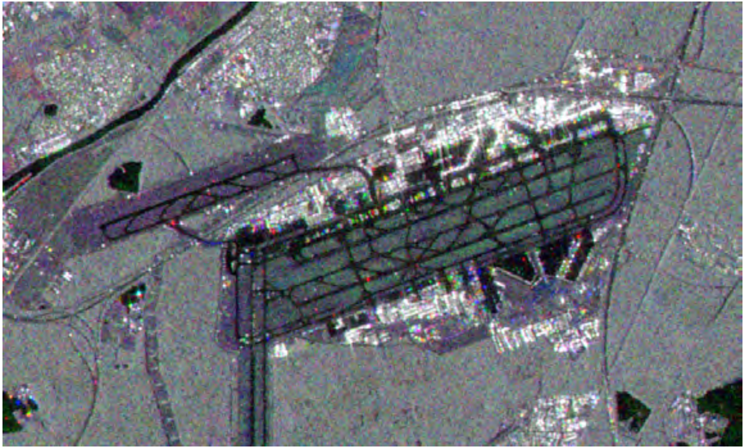

RGB image of Sentinel-1 C-band multi-temporal VV data, 5 Mar 2016 as B, 15 Jul 2016 as G, and 31 Oct 2016 as R, 10 m pixels, 6 km north-south and 10 km east-west. -24 dB $\rightarrow$ 6 dB.

Results, test statistic

$-2 \ln Q$ omnibus change detector for Sentinel-1 C-band VV/VH dual polarization data, diagonal only, stretched linearly between 0 and 300.

Results, number of changes, R_j only

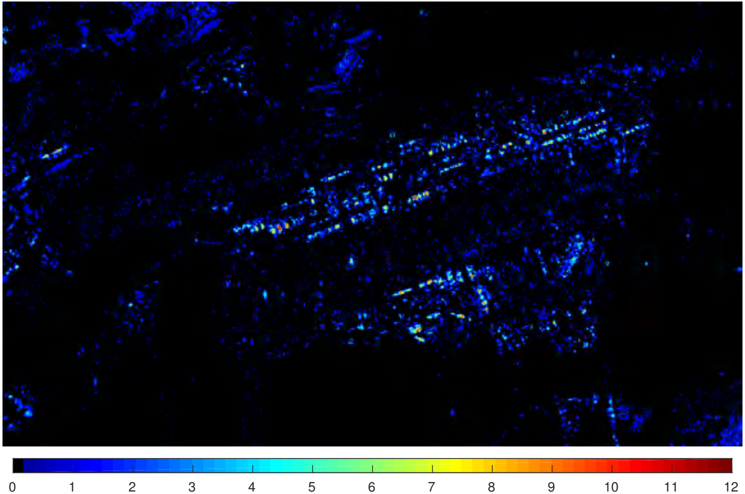

Results, number of changes, Q and R_j

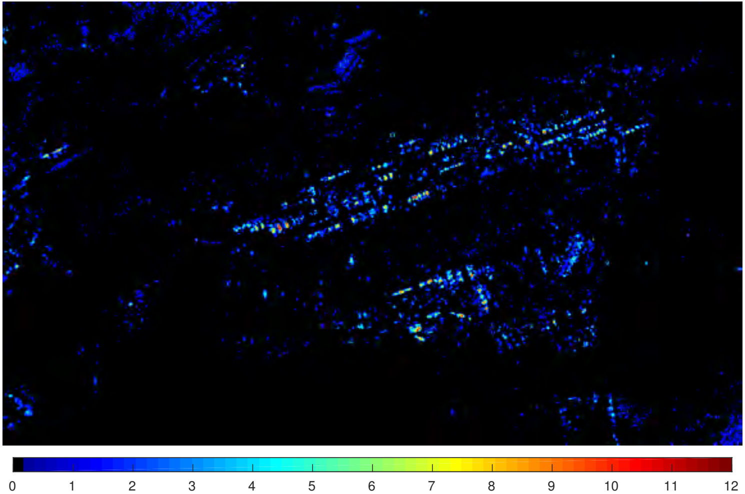

Results, first change

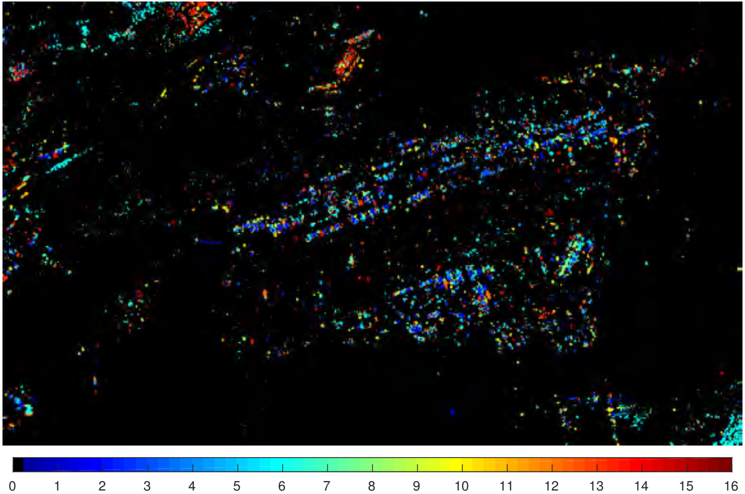

Results, last change

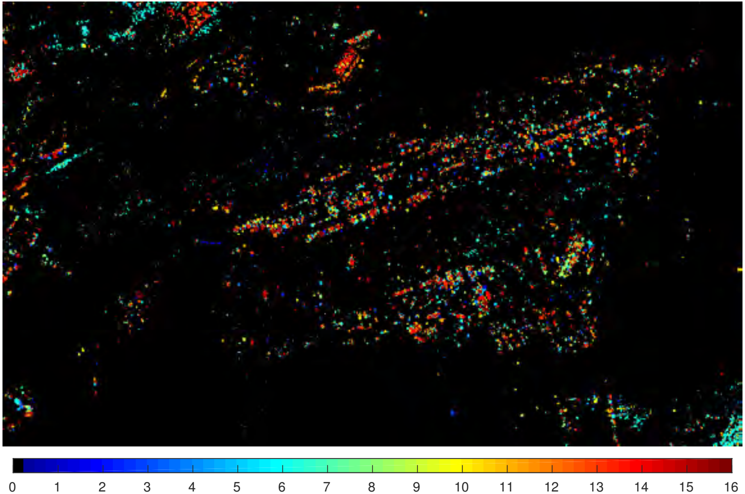

Results, maximum change

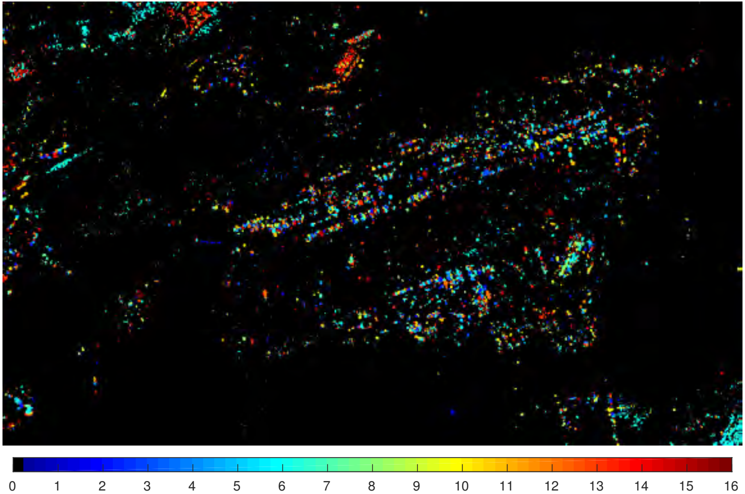

Results, RGB example

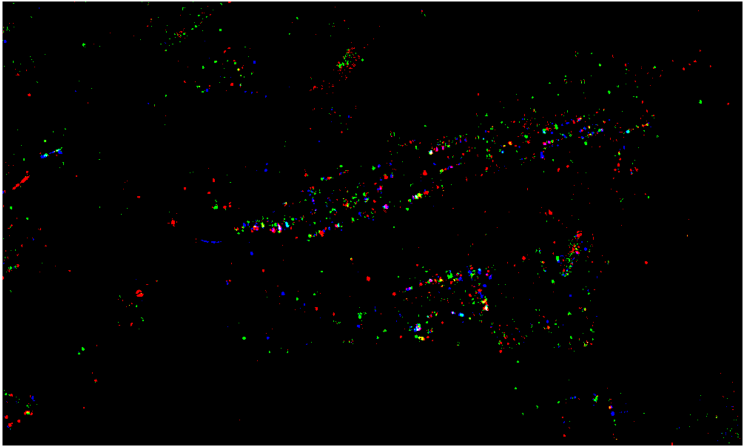

Change after 5 Mar 2016 is B, 15 Jul 2016 is G, and 19 Oct 2016 is R, 10 m pixels, 6 km north-south and 10 km east-west.

Results, RGB example in GE

Results, first 10 time points only

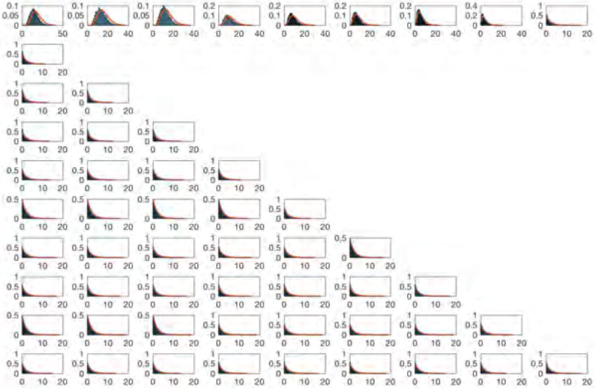

Histograms for an analysis of omnibus change for the first ten time points of the Sentinel-1 data (5 Mar through 27 Jul) along with the theoretical distributions for a no-change wooded area (top of image). For the $-2 \ln Q$ (top row plots) the numbers of degrees of freedom are 18, 16, ..., 2, respectively. For all the $-2 \ln R_j$ (the remaining rows) the number of degrees of freedom is 2. Judged visually this illustrates a satisfactory fit between sample histograms and theoretical distributions for the test statistics in a no-change region.

Results, first 10 of 19 time points

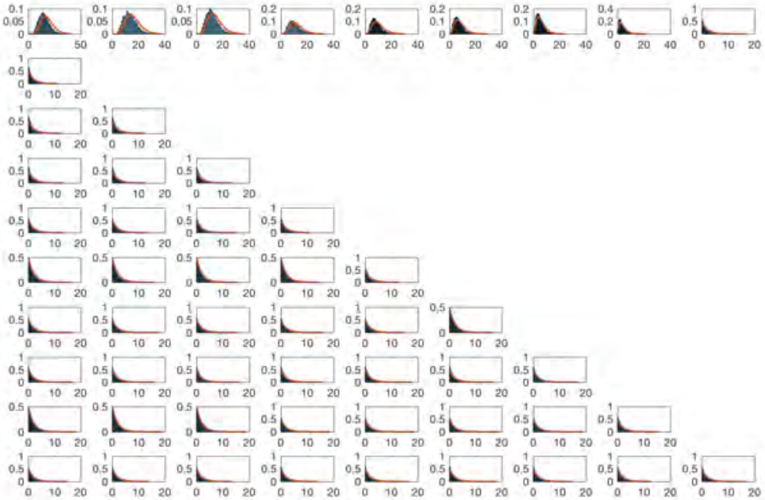

S-1, 28 scenes Apr–Dec 2016, port activity, GEE

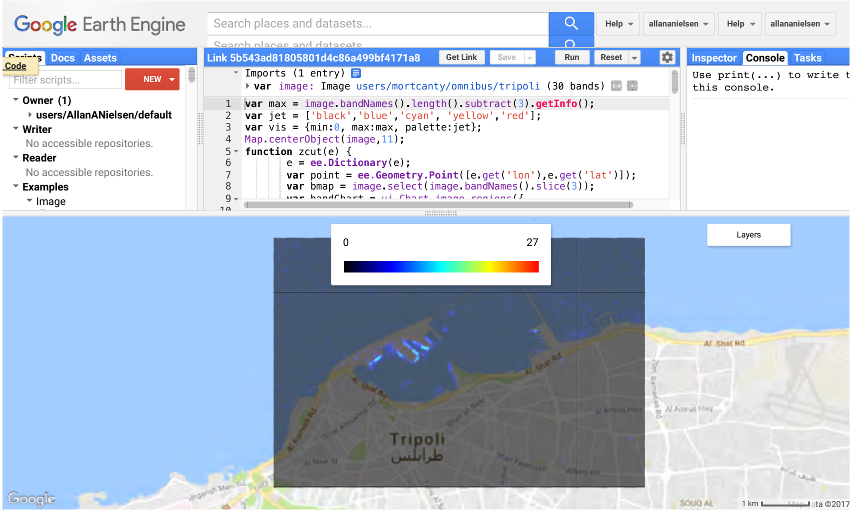

S-1, 19 scenes May–Oct 2016, agricultural activity, GEE

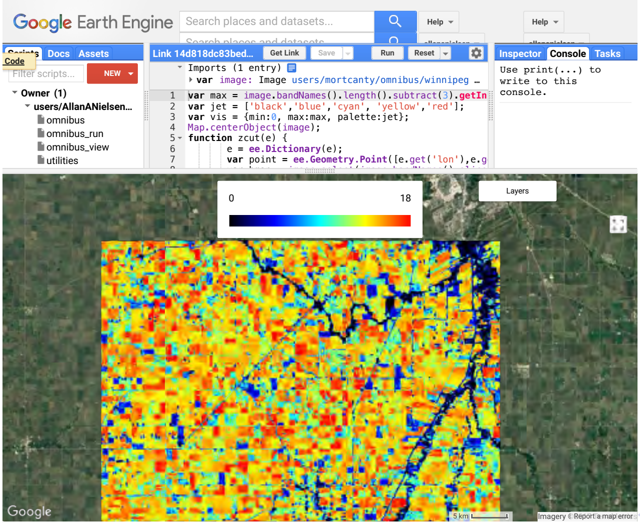

S-1, 19 scenes Apr–Oct 2017, hurricane Maria (20 Sep), GEE

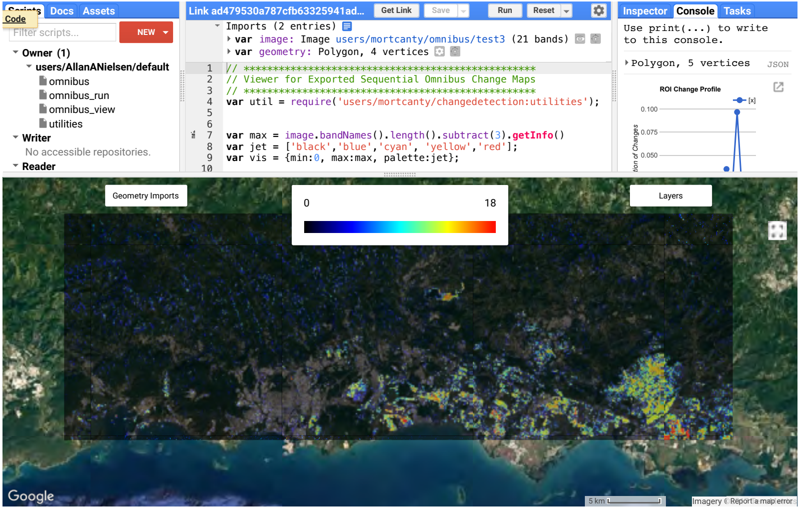

S-1, 19 scenes Apr–Oct 2017, hurricane Maria (20 Sep), GEE

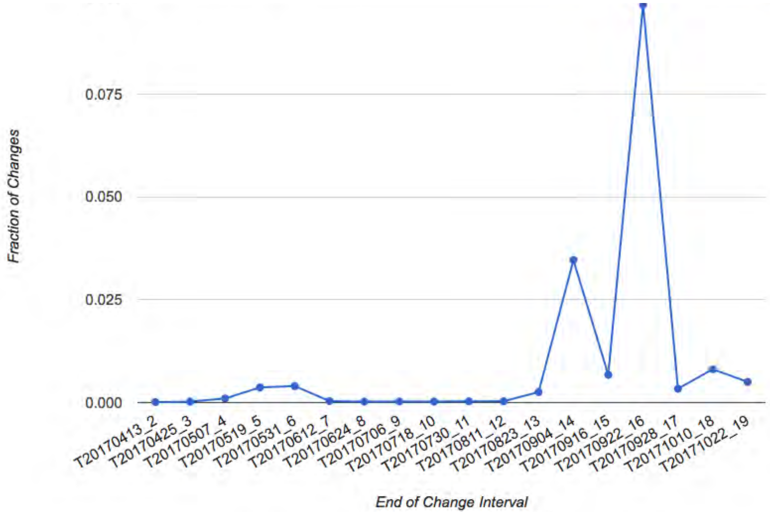

Software

- Matlab, lots of possibilities for small datasets, including automatic generation of tables, histogram/distribution plots, and visualizations[4].

[4] https://people.compute.dtu.dk/alan
[5] https://hub.docker.com/u/mort
[6] http://mortcanty.github.io/SARDocker
[7] http://mortcanty.github.io/src/tutorialsar.html
[8] https://github.com/mortcanty/earthengine

Software

- Matlab, lots of possibilities for small datasets, including automatic generation of tables, histogram/distribution plots, and visualizations[4].
- Matlab, line-by-line implementation for SAR.

[4] https://people.compute.dtu.dk/alan
[5] https://hub.docker.com/u/mort
[6] http://mortcanty.github.io/SARDocker
[7] http://mortcanty.github.io/src/tutorialsar.html
[8] https://github.com/mortcanty/earthengine

Software

- Matlab, lots of possibilities for small datasets, including automatic generation of tables, histogram/distribution plots, and visualizations[4].
- Matlab, line-by-line implementation for SAR.
- Python (IPython and Docker)[5,6,7].

[4] https://people.compute.dtu.dk/alan
[5] https://hub.docker.com/u/mort
[6] http://mortcanty.github.io/SARDocker
[7] http://mortcanty.github.io/src/tutorialsar.html
[8] https://github.com/mortcanty/earthengine

Software

- Matlab, lots of possibilities for small datasets, including automatic generation of tables, histogram/distribution plots, and visualizations[4].
- Matlab, line-by-line implementation for SAR.
- Python (IPython and Docker)[5,6,7].
- Google Earth Engine (GEE) on open-source repository Github[8]. Client-side programs run in a local Docker container serving a simple Flask web application. Docker engine plus browser needed (and authentication to GEE), nothing else.

[4] https://people.compute.dtu.dk/alan
[5] https://hub.docker.com/u/mort
[6] http://mortcanty.github.io/SARDocker
[7] http://mortcanty.github.io/src/tutorialsar.html
[8] https://github.com/mortcanty/earthengine

Software on GEE

- JavaScript code[9] to run the IR-MAD and the omnibus methods directly in the GEE code editor/playground. Omnibus code also generates MP4 movie showing where and when change occurred.

[9] http://fwenvi-idl.blogspot.de/
[10] http://www.imm.dtu.dk/pubdb/p.php?7024
[11] http://www.imm.dtu.dk/pubdb/p.php?7027

Software on GEE

- JavaScript code[9] to run the IR-MAD and the omnibus methods directly in the GEE code editor/playground. Omnibus code also generates MP4 movie showing where and when change occurred.
- Morton J. Canty and Allan A. Nielsen. Spatio-temporal analysis of change with Sentinel imagery on the Google Earth Engine. *ESA Conference on Big Data from Space*, pp. 126-129, Toulouse, France, 28-30 Nov 2017[10].

[9] http://fwenvi-idl.blogspot.de/
[10] http://www.imm.dtu.dk/pubdb/p.php?7024
[11] http://www.imm.dtu.dk/pubdb/p.php?7027

Software on GEE

- JavaScript code[9] to run the IR-MAD and the omnibus methods directly in the GEE code editor/playground. Omnibus code also generates MP4 movie showing where and when change occurred.
- Morton J. Canty and Allan A. Nielsen. Spatio-temporal analysis of change with Sentinel imagery on the Google Earth Engine. *ESA Conference on Big Data from Space*, pp. 126-129, Toulouse, France, 28-30 Nov 2017[10].
- Allan A. Nielsen, Knut Conradsen, Henning Skriver and Mort Canty (2017). Visualization of and software for omnibus test based change detected in a time series of polarimetric SAR data[11]. *Canadian Journal of Remote Sensing* **43**(6), 582-592. DOI:10.1080/07038992.2017.1394182.

[9] http://fwenvi-idl.blogspot.de/
[10] http://www.imm.dtu.dk/pubdb/p.php?7024
[11] http://www.imm.dtu.dk/pubdb/p.php?7027

Recent Software

- Docker-based interface to the GEE for the Wishart omnibus algorithm[12] (flexible, via Jupyter notebook).

[12] http://fwenvi-idl.blogspot.com/2018/07/jupyter-notebook-interfacefor.html/
[13] https://www.databio.eu
[14] https://github.com/BehnazP/DataBio/

Recent Software

- Docker-based interface to the GEE for the Wishart omnibus algorithm[12] (flexible, via Jupyter notebook).
- Computer implementation work within the Horizon 2020 project DataBio[13] DLV-732064 funded by the European Union: command-line and GUI executables[14] for Windows and Linux, version for small images which fit into memory and a line-by-line version for big data (BiDS 2019 poster #13, Dr Behnaz Pirzamanbein).

[12] http://fwenvi-idl.blogspot.com/2018/07/jupyter-notebook-interfacefor.html/

[13] https://www.databio.eu

[14] https://github.com/BehnazP/DataBio/

Conclusions

- CCA based automatic change detection and automatic normalization in bitemporal multispectral optical data (Sentinel-2 MSI and Landsat TM).

Conclusions

- CCA based automatic change detection and automatic normalization in bitemporal multispectral optical data (Sentinel-2 MSI and Landsat TM).
- Omnibus Wishart distribution based automatic change analysis in multitemporal polarimetric SAR data (Sentinel-1).

Conclusions

- CCA based automatic change detection and automatic normalization in bitemporal multispectral optical data (Sentinel-2 MSI and Landsat TM).
- Omnibus Wishart distribution based automatic change analysis in multitemporal polarimetric SAR data (Sentinel-1).
- Computer implementations, including cloud versions.

Conclusions

- CCA based automatic change detection and automatic normalization in bitemporal multispectral optical data (Sentinel-2 MSI and Landsat TM).
- Omnibus Wishart distribution based automatic change analysis in multitemporal polarimetric SAR data (Sentinel-1).
- Computer implementations, including cloud versions.
  - GEE gang very helpful (Noel Gorelick, Simon (Vsevolod) Ilyushchenko), implemented incomplete gamma function, re-ingest all S-1 data (store in floats rather than 2-byte int "clamped to the 1st and 99th percentile").

Conclusions

- CCA based automatic change detection and automatic normalization in bitemporal multispectral optical data (Sentinel-2 MSI and Landsat TM).
- Omnibus Wishart distribution based automatic change analysis in multitemporal polarimetric SAR data (Sentinel-1).
- Computer implementations, including cloud versions.
  - GEE gang very helpful (Noel Gorelick, Simon (Vsevolod) Ilyushchenko), implemented incomplete gamma function, re-ingest all S-1 data (store in floats rather than 2-byte int "clamped to the 1st and 99th percentile").
- Use software, read and cite our (journal) papers.

Cloud based spatio-temporal analysis of change in sequences of Sentinel images

Allan A. Nielsen[1], Morton J. Canty[2], Henning Skriver[1], Knut Conradsen[1]

[1]Technical University of Denmark
[2]Research Center Jülich, Germany

ESA Big Data from Space, Munich, Germany, 19-21 Feb 2019